The Astrophysical Journal, 869:169 (8pp), 2018 December 20 https://doi.org/10.3847/1538-4357/aaf797

Vortex Flows in the Solar Atmosphere: Automated Identification and Statistical Analysis

Ioannis Giagkiozis[1], Viktor Fedun[2], Eamon Scullion[3], David B. Jess[4], and Gary Verth[5]
[1] School of Mathematics and Statistics, University of Sheffield, Hicks Building, Hounsfield Road, Sheffield, S3 7RH, UK
[2] Plasma Dynamics Group, Automatic Control and Systems Engineering Department, University of Sheffield, Amy Johnson Building, Mappin Road, S1 3JD, UK
v.fedun@sheffield.ac.uk
[3] Department of Mathematics, Physics and Electrical Engineering, Northumbria University, Newcastle upon Tyne, UK
[4] Astrophysics Research Centre, School of Mathematics and Physics, Queen's University Belfast, Belfast, BT7 1NN, UK
[5] Plasma Dynamics Group, School of Mathematics and Statistics, University of Sheffield, Hicks Building, Hounsfield Road, Sheffield, S3 7RH, UK
Received 2018 May 25; revised 2018 December 5; accepted 2018 December 7; published 2018 December 26

Abstract

Vortices on the photosphere are fundamentally important as these coherent flows have the potential to form coherent magnetic field structures in the solar atmosphere, e.g., twisted magnetic flux tubes. These flows have traditionally been identified by tracking magnetic bright points (BPs) using primarily visual inspection. This approach has the shortcoming that it introduces bias into the statistical analyses. In this work we fully automate the process of vortex identification using an established method from hydrodynamics for the study of eddies in turbulent flows. For the first time, we apply this to detect intergranular photospheric intensity vortices. Using this automated approach, we find that the expected lifetime of intensity vortices is much shorter (≈17 s) compared with previously observed magnetic BP swirls. We suggest that at any time there are 1.48×10^6 such small-scale intensity vortices covering about 2.8% of the total surface of the solar photosphere. Lastly, we compare our results with previous works and speculate what this could imply with regards to estimating the global energy flux due magnetic tornadoes in the solar atmosphere with future higher resolution instrumentation.

Key words: Sun: atmosphere – Sun: oscillations – Sun: photosphere

Supporting material: animation

1. Introduction

Traditionally photospheric intensity flow fields have been traced using local correlation tracking of (magnetic) bright points (BPs) and the revealed vortex flows have been identified by eye. This manual approach has two major shortcomings: (i) it introduces observational bias into the statistical analysis and (ii) a large number of vortex flow fields are most likely missed simply due to the sheer scale of the task, which also has adverse effects on the variance of the statistical analysis. Small-scale vortices in the quiet Sun regions are widely accepted to form due to turbulent convection and the bathtub effect (e.g., Shelyag et al. 2011; Kitiashvili et al. 2012a; Shelyag et al. 2012). Solar photospheric vortex flows have drawn the attention of researchers as they have the potential to excite a wide range of magnetohydrodynamics (MHD) waves, e.g., slow and fast magneto-acoustic as well as Alfvén (Fedun et al. 2011; Mumford et al. 2015; Mumford & Erdélyi 2015). Vortex flows also appear to have a prominent role in both direct and alternating current models of solar atmospheric heating. In direct current models, neighboring magnetic flux tubes (or strands) can become magnetically twisted under the influence of photospheric vortices. This, in turn, implies that current sheets may develop at the interface between such strands allowing the possibility of magnetic reconnection (Parker 1972, 1983a, 1983b; Klimchuk 2015). In alternating current models, photospheric vortices can be seen as MHD wave drivers (Fedun et al. 2011; Mumford et al. 2015; Mumford & Erdélyi 2015) and as precursors to large-scale solar tornadoes (Wedemeyer-Böhm et al. 2012; Wedemeyer et al. 2013; Amari et al. 2015). These tornadoes have an estimated net positive Poynting flux of 440 W m^{-2}, which is more than adequate to heat the quiet solar corona whose energy flux requirement is estimated to be approximately 300 W m^{-2} (Withbroe & Noyes 1977).

Unfortunately, despite the increasing interest in these coherent flows in the solar photosphere, the majority of previous observations provide relatively small sample sizes of such phenomena. For example, the work of Steiner et al. (2010), Palacios et al. (2012), and Park et al. (2016) only document a few isolated events, while the results of Bonet et al. (2008, 2010) and Vargas Domínguez et al. (2011) push this limit to a few tens of detected events. On the other hand, existing vortex identification methods (e.g., Moll et al. 2011; Kato & Wedemeyer 2017; Rempel et al. 2017) have been successfully applied to numerical simulations of the solar atmosphere, where all components of the velocity and magnetic fields are known with a high degree of precision.

In this paper we present a fully automated method to identify vortex flows, namely the center of circulation and their flow boundary that is based on local correlation tracking (Fisher & Welsch 2008) applied to photospheric intensity observations, combined with an established method for identifying vortices used in the study of turbulence (Graftieaux et al. 2001). Subsequently, we estimate characteristic vortex parameters, such as lifetime, diameter, mean perpendicular velocity, and area. The main results of this paper are as follows. There is an abundance of small-scale intensity vortices in the quiet Sun and their typical lifetimes are approximately 17 s. We estimate that at any given time, the expected number of vortices in the photosphere is 1.4×10^6 and that they occupy 2.8% of the photosphere. Although the area of these vortices may appear

small in the photosphere, even if only a tenth of these vortex flows reach the lower corona, they may occupy more than 17% of its total area.

2. Observations and Vortex Identification Process

2.1. Observations

The observations investigated here were carried out between 08:07:24 and 09:05:46 UT on 2012 June 21 with the CRisp Imaging SpectroPolarimeter (CRISP) at the Swedish 1-m Solar Telescope (SST; Scharmer et al. 2003, 2008) on La Palma. The image scale of the CRISP observations is $0\farcs059$ per pixel. A quiet Sun region very close to the disk center was observed with an effective field of view of 55×55 arcsec, centered on solar-$x = -3\farcs1$ and solar-$y = 69\farcs9$. The spectropolarimetric sequences have a post-reduction mean cadence of 8.25 s. After acquisition, the data was processed with the Multi-Object Multi-Frame Blind Deconvolution (MOMFBD) algorithm (van Noort et al. 2005; van Noort & Rouppe van der Voort 2008; de la Cruz Rodríguez et al. 2015).

2.2. Vortex Identification Process

The automated vortex identification methodology we present splits into four stages: (i) preprocessing, (ii) velocity field estimation, (iii) vortex identification, and (iv) vortex lifetime estimation. The intensity maps obtained from observations have varying intensity at different times, which appears to be due to atmospheric effects. These intensity variations are a few standard deviations from the mean and the effect is global. To counter these effects image histogram equalization (e.g., Pizer et al. 1987) was used as follows.

1. First, the expected distribution of intensities is estimated by means of averaging the histogram distributions across all of the frames. The rationale for this is that the Sun is not expected to change its general power emission spectrum during the time of the observation.
2. Once the expected intensity distribution has been obtained, histogram equalization is applied to all of the frames using that distribution as a reference.

This procedure is fast and efficiently removes interframe flickering, and, improves the numerical stability of the local correlation tracking (LCT) method.

The preprocessing stage removes rapid intensity fluctuations while preserving the relative counts as much as possible. Subsequently, we remove the subtle variability in the seeing conditions over time in our observations using a moving average Gaussian filter. Although it is well known that atmospheric seeing is a nonlinear effect (see, e.g., November & Simon 1988), given that the seeing conditions were good, this simple averaging method produced similar results to destreching algorithms and is computationally more efficient. To avoid the reduction of the temporal resolution, this moving average Gaussian filter is employed with a 3 dB attenuation at a quarter of the Nyquist frequency $1/(8T)$, where T is the cadence. This Gaussian filter is a low-pass filter with a passband of $(0, 1/4f_{\mathrm{N}})$, where f_{N} is the Nyquist frequency, which is one-half that of the sampling frequency f_S. The benefit of filtering the signal is that aliasing effects, which are often present in sampled signals, are reduced. The use of this filter is motivated by the prevalence of short lived vortices and we need to make sure that this is not a side effect of noise in the signal. In fact, we find that filtering only has a small impact on the estimated lifetimes of the vortices, which gives us more confidence in our results. At the same time, the employed moving average Gaussian filter has a finite impulse response and therefore can be constructed with only a small number of parameters (lags), which means that the number of samples (images) is not reduced as much as with other filters. To achieve the bandpass characteristics $(0, 1/4f_{\mathrm{N}})$ we need, the Gaussian filter needs only five parameters, meaning that we lose only four images from the entire set. The velocity field estimation is performed using Fourier local correlation tracking (Fisher & Welsch 2008) with a Gaussian apodizing window with a width of $\sigma = 10$ pixels (Louis et al. 2015).

Subsequently, for the vortex identification, we implement a proven and established method from the study of turbulence in fluid dynamics. Once the velocity field estimates are found, we implement the same approach as Graftieaux et al. (2001) to identify the vortex centers and boundaries. Graftieaux et al. (2001) defined two functions, Γ_1 and Γ_2, for the identification of the vortex centers and boundaries, respectively. In this paper we use the discrete version of both functions. The function Γ_1 used in this work is

$$\Gamma_1(\boldsymbol{x}_p) = \frac{1}{N}\sum_{S}\frac{((\boldsymbol{x}_m - \boldsymbol{x}_p)\times \boldsymbol{v}_m)\cdot \mathbf{1}_z}{||\boldsymbol{x}_m - \boldsymbol{x}_p||_2 \cdot ||\boldsymbol{v}_m||_2}. \tag{1}$$

Here, $S = \{\boldsymbol{x}_m : \ ||\boldsymbol{x}_m - \boldsymbol{x}_p||_2 \leqslant R\}$ is a disk of radius R about point $\boldsymbol{x}_p$, N is the number of pixels within a distance R of point $\boldsymbol{x}_p$, $||\cdot||_2$ is the Euclidean norm, $\mathbf{1}_z$ is a unit vector normal to the plane, and $|S|$ is the cardinality of S. Γ_1 defines a scalar field and its magnitude achieves a maximum at unity. Graftieaux et al. (2001) shows that this function achieves this maximum when $\boldsymbol{x}_p$ is at the center of an axisymmetric vortex. However, given that ideal axisymmetric vortices are quite uncommon, the threshold for classifying a point in S as a potential vortex center is reduced to 0.9, and, the local maximum of these points is classified as the vortex center. For the identification of the vortex boundary, we use Γ_2, defined as

$$\Gamma_2(\boldsymbol{x}_p) = \frac{1}{N}\sum_{S}\frac{((\boldsymbol{x}_m - \boldsymbol{x}_p)\times (\boldsymbol{v}_m - \bar{\boldsymbol{v}}_p))\cdot \boldsymbol{I}_z}{||\boldsymbol{x}_m - \boldsymbol{x}_p||_2 \cdot ||\boldsymbol{v}_m - \bar{\boldsymbol{v}}_p||_2}, \tag{2}$$

where $\bar{\boldsymbol{v}}_p$ is the average convective velocity around point $\boldsymbol{x}_p$. For a forced vortex, azimuthal velocity will increase radially from the vortex core to the boundary then decay radially with distance from the boundary. Hence, this velocity component has a maximum at the boundary. In Equation (2), by subtracting the average convective velocity both inside and outside the vortex boundary from the quantity $\boldsymbol{v}_m$, along with the cross-product, helps pinpoint the region of the maximum azimuthal velocity, i.e., the vortex boundary. It is shown in Graftieaux et al. (2001) that in the inner core of a vortex the magnitude of Γ_2 is larger than $2/\pi$. Flows with values of $\Gamma_2 < 2/\pi$ are dominated by strain and when $\Gamma_2 = 2/\pi$, we have a pure shear. In the limit of small S the quantity Γ_2 depends on (i) the rotation rate (Ω) of the antisymmetric part of the velocity gradient at point P and (ii) the eigenvalue (μ) of the symmetric part of this tensor (which is equivalent to the derivative of the strain rate tensor). Hence the ratio Ω/μ indicates whether rotation or strain is dominating or if there is pure shear flow as shown in Graftieaux et al. (2001).

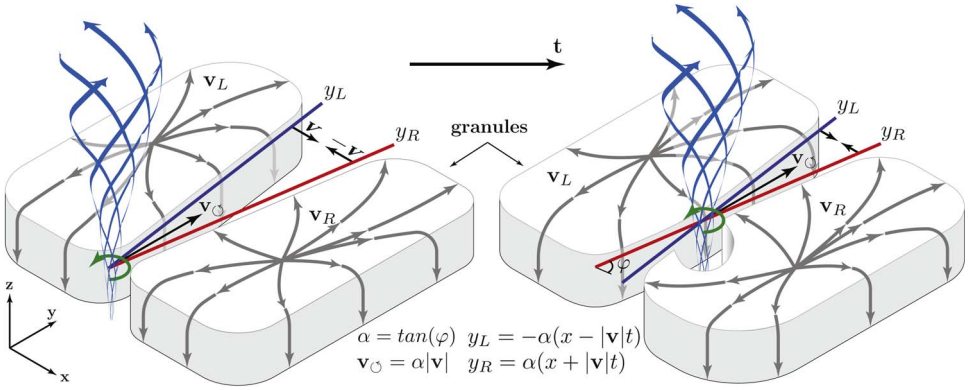

Figure 1. Cartoon of the proposed physical mechanism modeling the high velocity of the vortex centers. The line segments y_L and y_R shown in blue and red, respectively, represent the edges of the two neighboring granules. In this instance, the two edges are moving toward each other with speed $|\boldsymbol{v}|$, which in general is not observed to be supersonic. The streamlines in the plane outline the velocity field near the edges of the granules, with $\boldsymbol{v}_L$ and $\boldsymbol{v}_R$ denoting the velocity field in the left and right granule, respectively. The velocity of the vortex center is labeled $\boldsymbol{v}_\circlearrowleft$, which due to the scaling factor α, may be supersonic. The blue streamlines in the z-direction depict magnetic field lines above the vortex center. The black arrow shows the evolution.

Let us now calculate the vortex centers and their boundaries at every time instance, however, we still need to estimate the lifespan of these vortices. For this purpose we assume that the vortex center can move at approximately the sound speed of the photosphere, about 10 km s^{-1} (Nordlund et al. 2009). If the speed of the vortex center is comparable to the sound speed, this would suggest that the maximum distance a center could traverse from one frame to the next would be 82.5 km, which is almost 2 pixels at the spatial resolution of our data. However, at present the vortex formation mechanism has not been clearly established and if such flows in the photosphere are formed as shown in Figure 1, the speed of their center may be much larger than the sound speed. What we suggest in Figure 1 is the following. The edges of the granules are represented as line segments (red and blue line segments in Figure 1). We define the points where the vertical component of the velocity transits from being mostly positive, as it is on granules, to being negative, as is the case in the intergranular lanes.

Due to the dynamic nature of the granulation pattern on the photosphere, their edges are in constant relative motion with respect to the edges of neighboring granules. This relative motion, when combined with counter streaming flows of two neighboring granules, can drive vortex flows whose centers can move ($\boldsymbol{v}_\circlearrowleft$) at a much larger speed compared with the relative speed that generated them (see Figure 1). Therefore, using a conservative estimate, we assume that vortices that are within a 4 pixel radius in two consecutive times are, in fact, the same vortex.

3. Results and Statistical Analysis

A representative example of the results obtained from the vortex identification process is shown in Figure 2. The gray scale denotes intensity, normalized in the range 0–1 corresponding to black and white, respectively. Overplotted is the LCT estimate of the surface velocity field. The red filled circles mark the counterclockwise vortex flows (positive), the blue circles correspond to the clockwise flows (negative), and the orange line delimits the vortex flow boundary.

Figures 3 and 4 show the statistical results based on a sample size of $N = 26,988$ vortices. As the only source of information that is used here is based on LCT applied to intensity observations, we refer to the identified vortex flows as intensity vortices. This is to acknowledge the line-of-sight integration effects and temperature variations that, from a practical standpoint, lead to the estimated velocity field being a weighted average of the plasma motions at different heights within the spectral line formation height.

We find that the expected lifetime of such vortices is independent of orientation (see (a) and (b) in Figure 3). In fact, we have found no statistically significant deviations in the distributions of positively or negatively oriented vortices for any of the measured parameters, i.e., lifetime, space and time density, diameter, area, or perpendicular speed (see Figures 3 and 4). What is intriguing, however, is that for the majority of vortices (approximately 85%), their expected lifetimes are less or equal to three times the cadence (24.75 s). This is much shorter when compared with similar features identified by tracking magnetic BPs (e.g., Bonet et al. 2008). The apparent discrepancy could be attributed to errors in LCT, where very short lived structures are the result of errors in the identified velocity field. Notwithstanding this limitation, LCT velocity maps have been shown to be a reasonable first order approximation to the velocity field (Verma et al. 2013; Louis et al. 2015). These authors did this analysis using MHD convection simulation data, where the actual horizontal velocity field components were known to a high accuracy. However, in the computational domain of Louis et al. (2015), there were both regions between granules and on granules where there was a notable difference between the LCT results and the actual velocity field. This is shown in Figures 5 and 6 of their paper. On the other hand, there are also regions between granules which show a good correspondence. Since the exact physical connection between vortices observed with intensity and the actual velocity flow field is currently not well understood, in the present work, we are calling the detected vortices intensity vortices to make this distinction clear.

Assuming an expected lifetime, for both positive and negative vortices of $\tau = 0.29$ minute (see (a)–(b) in Figure 3) and the space and time density of vortices of $d = 0.84$ Mm s^{-2} minute^{-1} (see (e) in Figure 3), we estimate that there will be $\tau \cdot d = 0.244$ Mm s^{-2} vortices at any given time. If the vortex parameters measured here remain consistent across the entire solar surface, this would imply that there are 1.48×10^6 vortices existing at any one time.

Figure 4 panels (e) and (f) show the distribution of the average perpendicular speed within the vortex boundary. This

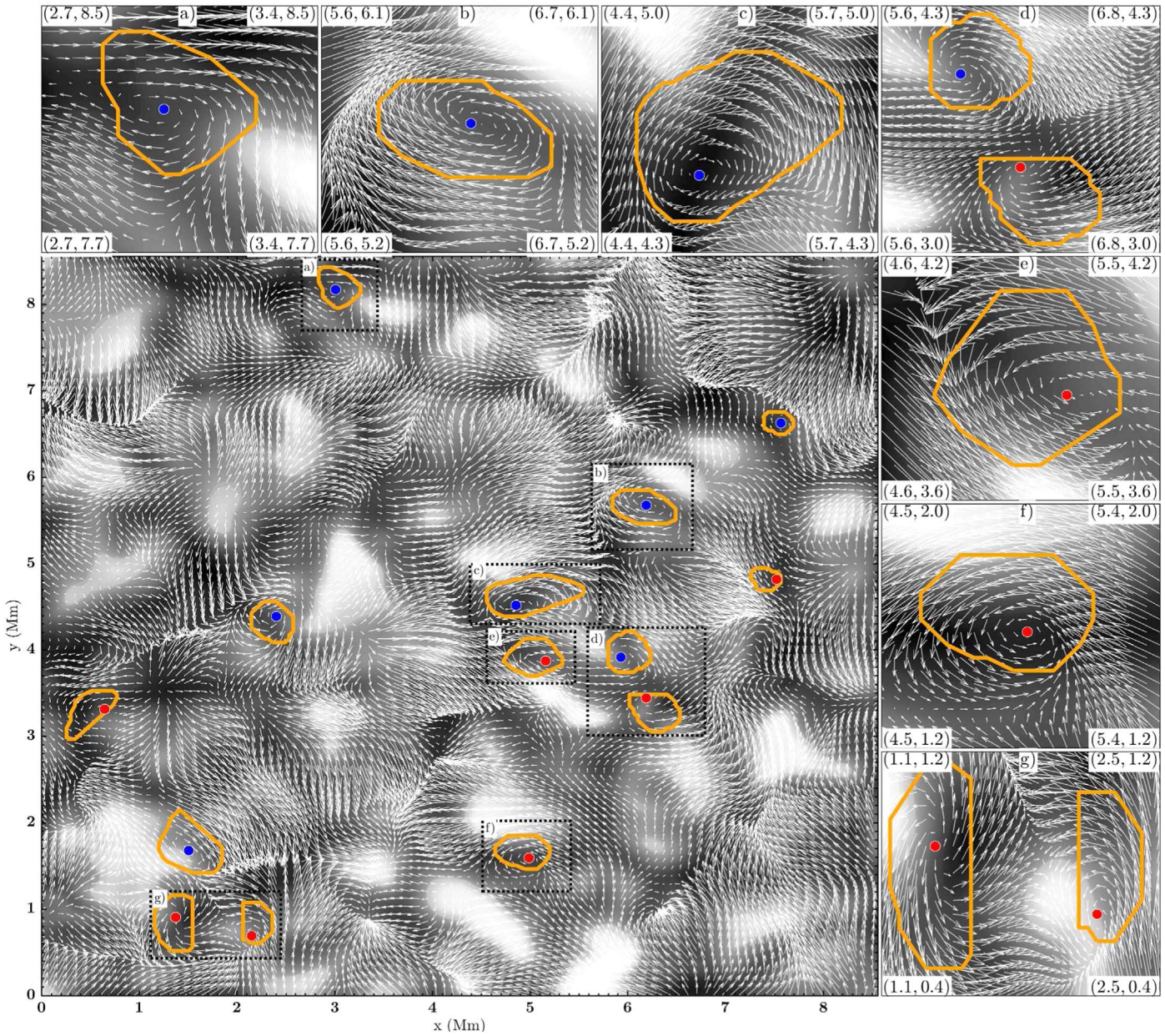

Figure 2. Snapshot of the estimated velocity field based on the Fe I continuum (intensity shown in gray scale) using LCT, illustrating the identified vortices and their boundaries. The circles denote the vortex center, with the red circles referring to the counterclockwise vortices (positive) and the blue circles to the clockwise vortices (negative). The orange border line denotes the vortex boundary. An animation of this figure is available. The video begins at $t = 8.25$ s and ends at $t = 3465.0$ s. The duration is 52 s.

(An animation of this figure is available.)

is calculated by projecting the velocity vector at every point within the vortex to a vector perpendicular to the ray emanating from the vortex center. Lastly, panel (g) in Figure 4 provides an estimate of the percent of the area of the photosphere covered by intensity vortices at any given time.

4. Discussion and Conclusions

Vortex flows in the solar atmosphere may contribute significantly to the energy flux requirements for heating the quiet Sun atmosphere. However, for that connection to be established strong evidence is required: (i) vortex flow motions are ubiquitous in the solar atmosphere and (ii) that these motions appear at different heights, e.g., the photosphere, chromosphere, and corona. We have shown that the automated identification approach described in this work results in a significantly larger number of identified vortices compared with previous observational studies. This is evidence consolidating the fact that small-scale vortices are prevalent in the solar photosphere. Most interestingly, an overwhelming majority of these vortices have lifetimes that are often much shorter than previously believed, which suggest that these flows are highly dynamic in nature.

Due to the episodic nature of the formation of these small-scale vortices, any magnetic field through them will be supplied with a broadband impulse comprised of both torsional and radial components, which will generate propagating MHD waves. The presence of a magnetic field in vortices is

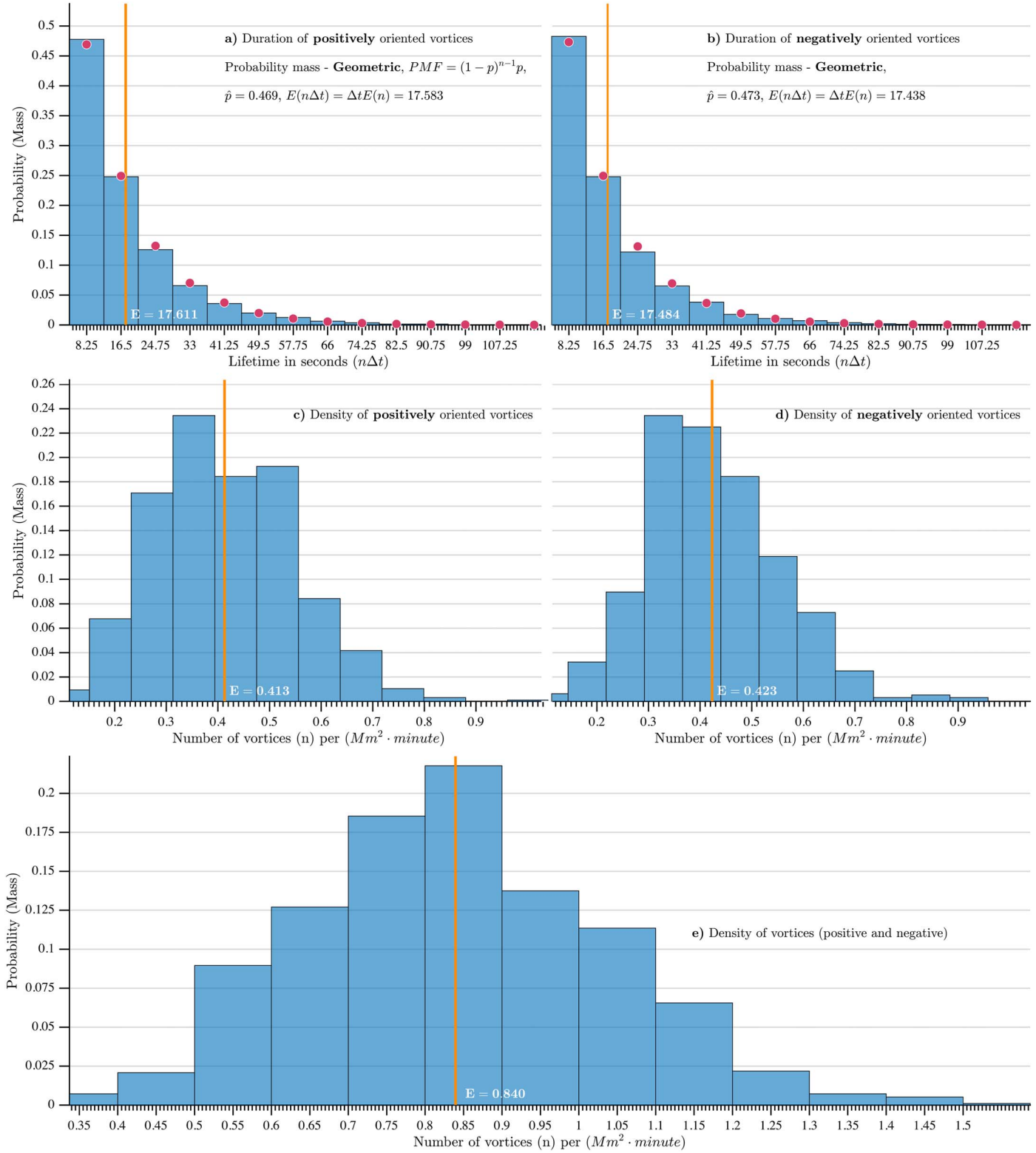

Figure 3. Estimates of (a) and (b) vortex lifetime mass functions, and (c), (d), and (e) are the number of vortices per $Mm^2 \cdot$ minute. The red circles denote the best fit of a parametric mass density function (PMF). In this case, the geometric distribution was a best fit for the lifetimes of the vortices. The orange line, as well as the white font E on its right, is the expected value calculated from the empirical distribution of the data. Values with a hat indicate the best-fit parameter estimates for the particular distribution, and, $E(\cdot)$ is the expected value.

consistent if we recall that their location is in the intergranular lanes where the magnetic field concentrations are highest. Both observational and numerical simulations (e.g., Fedun et al. 2011; Mumford et al. 2015; Mumford & Erdélyi 2015) support the idea that MHD waves with a broad frequency range can be generated by vortex flows. However this is to be expected on more fundamental grounds due to a particular duality in frequency space. Namely, localization in time leads to a spread

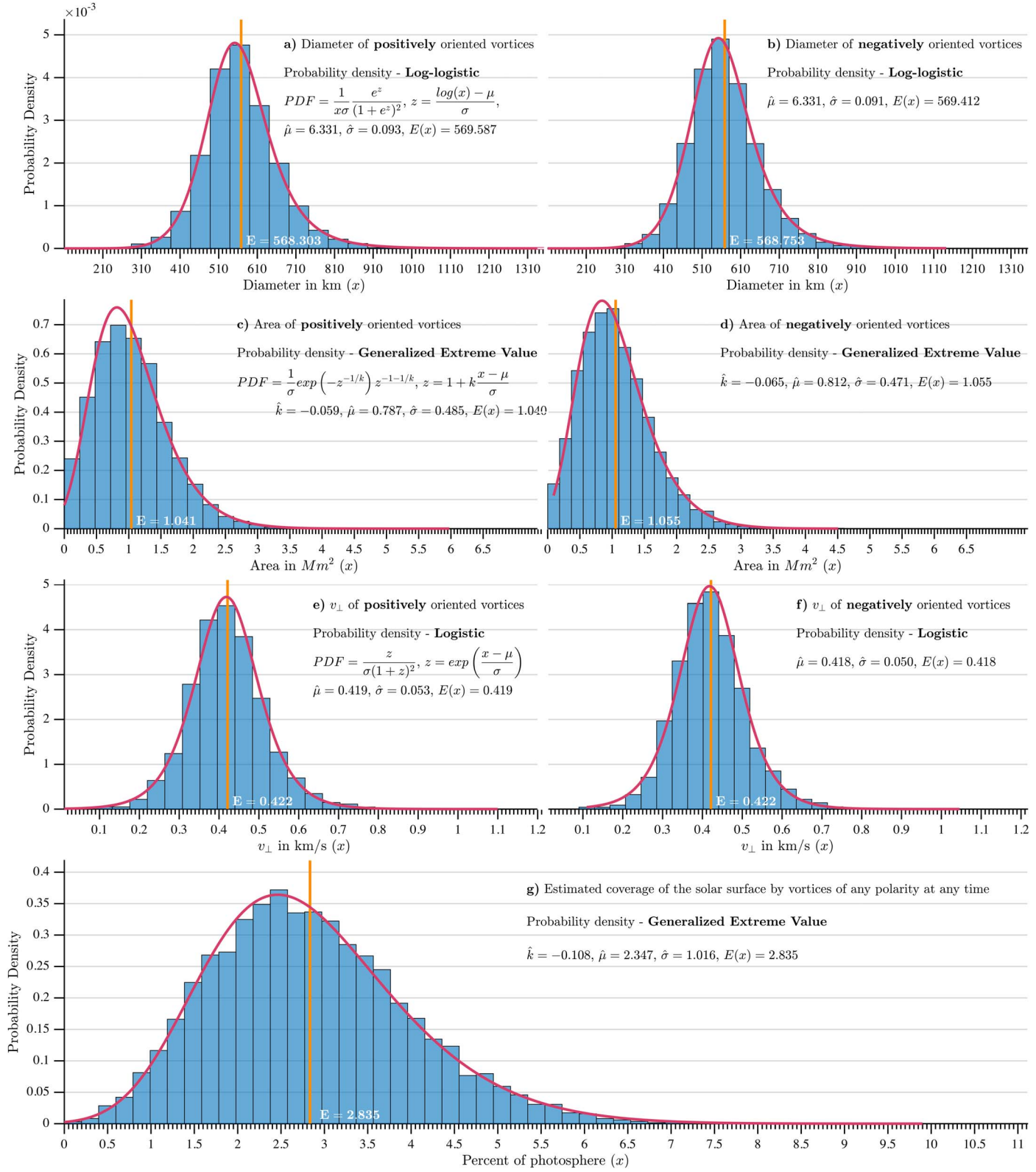

Figure 4. Empirical and parametric estimates of the probability density function (PDF) for (a) and (b) of the vortex diameter, which are calculated using the average of the minor and major axes of a best-fit ellipse for every vortex, (c) and (d) are the area of vortices (in Mm^2), (e) and (f) are the magnitude of the perpendicular velocity ($|v_\perp|$), and lastly, (g) is an estimate of the percentage of the total photosphere covered with intensity vortices. The notation in this figure follows that in Figure 3.

(broadening) in the frequency domain and vice versa. In physical terms this implies that the rapidity of vortex formation alongside with deviation from axis symmetry offer a wave driver that results in waves of different frequencies, albeit with different amplitudes. Regarding energy transport to the upper layers of the atmosphere, numerical simulations suggest that vortex driven MHD waves (Amari et al. 2015) are a feasible mechanism.

Table 1
Summary Statistics Comparing the Main Results in This Work with Previous Studies

	d (Mm^{-2} $minute^{-1}$)	τ (minute)		$E(\#)$ on Photosphere	Sample Size
Present work	0.84	0.29	0.244	1.48×10^6	26,988
Bonet et al. (2008)	1.8×10^{-3}	5.1	0.92×10^{-2}	0.55×10^5	138
Bonet et al. (2010)	3.1×10^{-3}	7.1	2.2×10^{-2}	1.3×10^5	42
Vargas Domínguez et al. (2011)	1.6×10^{-3}	15	2.4×10^{-2}	1.46×10^5	144
Wedemeyer-Böhm et al. (2012)	(1.4×10^{-4})	(12.7)	(1.8×10^{-3})	(1.1×10^4)	(14)

Note. Summary statistics of space and time density (d), expected lifetime (τ), number of vortices per Mm^{-2} ($\tau \cdot d$), and the expected number of vortices on the solar photosphere ($E(\#)$). In the last column we also provide the number of vortices on which the statistical analysis is based on. The values in the last row of the table are in parentheses as they do not correspond to observations in the photosphere; however, these are included for reference.

The most compelling differences compared with previous reports (e.g., Bonet et al. 2008, 2010; Vargas Domínguez et al. 2011) are in the expected lifetime and space and time density. Table 1 shows summary statistics comparing the main results in this work with previous studies that are based on more than three to four observed vortices. In our view, there are at least two explanations for this mismatch. First, vortex flows, and any type of feature tracking in observations, are time consuming and error prone when performed manually. This increases the likelihood of bias and increased variance. Also our estimate of lifetimes relies on the accuracy of LCT for the surface velocity field identification, which although has been shown to have reasonable correlation with the true velocity field (Louis et al. 2015), is only a first approximation to small-scale motions in intergranular lanes. Notwithstanding this uncertainty, given that our chosen automated technique is straightforward to implement, the results can be cross-validated by other studies, which, in our view, is extremely important. Since the submission of this work, de Souze e Almeida Silva et al. (2018) have published a paper where the Lagrangian averaged vorticity deviation (LAVD) technique for vortex identification (Haller et al. 2016), initially employed in vortex detection in 3D numerical simulations of MHD dynamo (Rempel et al. 2017), was further developed. de Souze e Almeida Silva et al. (2018) performed a comparison between vortex identification methods, which are based on vorticity strength (Zhou et al. 1999), Γ detection (Graftieaux et al. 2001), and modified LAVD techniques, and have found that all of these techniques have their strengths and weaknesses. It is clear that further work is needed, especially in vortex boundary identification, to reduce false detections.

In Table 1 only the results of Wedemeyer-Böhm et al. (2012) are estimated from chromospheric and lower coronal observations. The rest are estimated from only photospheric data. It can be seen that there is an order of magnitude decrease in the number of vortices detected in the chromosphere and lower corona when compared to the photospheric results of Bonet et al. (2008, 2010) and Vargas Domínguez et al. (2011). Furthermore, when compared to the present work, this decrease is even more significant, i.e., by two orders of magnitude. Since all of these estimates very much depend of the resolution of the instruments used, these vortex numbers can only be taken as lower bounds.

However, it is still interesting to consider the fact that, currently, significantly more vortices have been detected in the photosphere than higher up in the chromosphere and lower corona. Physically, this could just be due to the fact that not all vortices rooted in the photosphere manage to penetrate to these higher altitudes. On the other hand, if the majority of the vortices detected in the photosphere do reach the chromosphere and lower corona, then the actual number of magnetic tornadoes estimated by Wedemeyer-Böhm et al. (2012) could be wrong by orders of magnitude. This would also mean that the total energy flux due to magnetic tornadoes over the entire lower corona could be significantly underestimated. In relation to the present work, even if only 10% of the vortices rooted in the photosphere penetrate into the lower corona, this has the extraordinary implication that at least 17% of the area of the lower corona is constantly supplied with a positive Poynting flux of $440\,W\,m^{-2}$, as opposed to 1.2% implied from Wedemeyer-Böhm et al. (2012). The assumptions in this estimate are that the photospheric vortices that do extend up to the lower corona have a mean radius of 1.5 Mm, their corrected expected number is 1.48×10^5 vortices at every time, i.e., 10% of our intensity vortices on the photosphere, instead of 1.1×10^4 (see Table 1), and that the average net positive Poynting flux in each magnetic tornado is $440\,W\,m^{-2}$.

This speculation may be exciting, however, at present we are far from establishing a link between intensity vortices and magnetic tornadoes. If intensity vortices are indeed closely correlated with the actual velocity field, then, based on the simulation results reported by Kitiashvili et al. (2012a, 2012b), we anticipate that their expected size will decrease with the advent of higher spatial resolution observations. Hence, these current energy flux estimates related to the observed magnetic tornadoes and number of vortices could be revised. A prime example of near future expected capability is the Daniel K. Inouye Solar Telescope whose visible broadband imager is planned to have spatial resolution of 16 km to 25 km per pixel, at 430.4 nm and 656.3 nm, respectively, and a cadence of 3.2 s (Berger & ATST Science Team 2013).

I.G. would like to thank the Faculty of Science in the University of Sheffield for the SHINE studentship. I.G., V.F., and G.V. thank the STFC and the Royal Society for the support received. V.F. and G.V. acknowledge the 2016 Sheffield International Mobility Scheme. E.S. thanks the support of STFC grant ST/L006243/1 in the preparation of this paper. D.B.J. would like to thank the STFC for an Ernest Rutherford Fellowship, in addition to Invest NI and Randox Laboratories Ltd. for the award of a Research & Development Grant (059RDEN-1). All of the authors would like to thank Matthias Rempel for the engaging discussions on this work. The Swedish 1-m Solar Telescope is operated on the island of La Palma by the Institute for Solar Physics of Stockholm University in the Spanish Observatorio del Roque de los

Muchachos of the Instituto de Astrofísica de Canarias. The authors wish to acknowledge the DJEI/DES/SFI/HEA Irish Centre for High-End Computing (ICHEC) for the provision of computing facilities and support. We also thank the anonymous referee whose comments helped us to improve the manuscript. The authors would like to thank the EAST-TAC, of the Leibniz-Institute for Solar Physics (Germany), for awarding observing time on the SST in 2012. The SST is operated on La Palma by the Institute for Solar Physics at Stockholm University (Sweden).

ORCID iDs

Ioannis Giagkiozis https://orcid.org/0000-0002-5521-2196
Viktor Fedun https://orcid.org/0000-0002-0893-7346
Eamon Scullion https://orcid.org/0000-0001-9590-6427
David B. Jess https://orcid.org/0000-0002-9155-8039
Gary Verth https://orcid.org/0000-0002-9546-2368

References

Amari, T., Luciani, J.-F., & Aly, J.-J. 2015, Natur, 522, 188
Berger, T. & ATST Science Team 2013, AAS Meeting, 44, 400.02
Bonet, J. A., Márquez, I., Sánchez Almeida, J., et al. 2010, ApJL, 723, L139
Bonet, J. A., Márquez, I., Sánchez Almeida, J., Cabello, I., & Domingo, V. 2008, ApJL, 687, L131
de la Cruz Rodríguez, J., Löfdahl, M. G., Sütterlin, P., Hillberg, T., & Rouppe van der Voort, L. 2015, A&A, 573, A40
de Souze e Almeida Silva, S., Rempel, E. L., Pinheiro Gomes, T. F., Requerey, I. S., & Chian, A. C.-L. 2018, ApJL, 863, L2
Fedun, V., Shelyag, S., Verth, G., Mathioudakis, M., & Erdélyi, R. 2011, AnGeo, 29, 1029
Fisher, G. H., & Welsch, B. T. 2008, in ASP Conf. Ser. 383, Subsurface and Atmospheric Influences on Solar Activity, ed. R. Howe et al. (San Francisco: CA), 373
Graftieaux, L., Michard, M., & Grosjean, N. 2001, MeScT, 12, 1422
Haller, G., Hadjighasem, A., Farazmand, M., & Huhn, F. 2016, JFM, 795, 136
Kato, Y., & Wedemeyer, S. 2017, A&A, 601, A135
Kitiashvili, I. N., Kosovichev, A. G., Mansour, N. N., Lele, S. K., & Wray, A. A. 2012a, PhyS, 86, 018403
Kitiashvili, I. N., Kosovichev, A. G., Mansour, N. N., & Wray, A. A. 2012b, ApJL, 751, L21
Klimchuk, J. A. 2015, RSPTA, 373, 20140256
Louis, R. E., Ravindra, B., Georgoulis, M. K., & Küker, M. 2015, SoPh, 290, 1135
Moll, R., Cameron, R. H., & Schüssler, M. 2011, A&A, 533, A126
Mumford, S. J., & Erdélyi, R. 2015, MNRAS, 449, 1679
Mumford, S. J., Fedun, V., & Erdélyi, R. 2015, ApJ, 799, 6
Nordlund, Å., Stein, R. F., & Asplund, M. 2009, LRSP, 6, 2
November, L. J., & Simon, G. W. 1988, ApJ, 333, 427
Palacios, J., Balmaceda, L. A., Domínguez, S. V., Cabello, I., & Domingo, V. 2012, in ASP Conf. Ser. 454, Hinode-3: The 3rd Hinode Science Meeting, ed. T. Sekii, T. Watanabe, & T. Sakurai (San Francisco, CA: ASP), 51
Park, S.-H., Tsiropoula, G., Kontogiannis, I., et al. 2016, A&A, 586, A25
Parker, E. N. 1972, ApJ, 174, 499
Parker, E. N. 1983a, ApJ, 264, 642
Parker, E. N. 1983b, ApJ, 264, 635
Pizer, S. M., Amburn, E. P., Austin, J. D., et al. 1987, CVGIP, 39, 355
Rempel, E. L., Chian, A. C.-L., Beron-Vera, F. J., Szanyi, S., & Haller, G. 2017, MNRAS, 466, L108
Scharmer, G. B., Bjelksjo, K., Korhonen, T. K., Lindberg, B., & Petterson, B. 2003, Proc. SPIE, 4853, 341
Scharmer, G. B., Narayan, G., Hillberg, T., et al. 2008, ApJL, 689, L69
Shelyag, S., Fedun, V., Erdélyi, R., Keenan, F. P., & Mathioudakis, M. 2012, in ASP Conf. Ser. 463, Second ATST-EAST Meeting: Magnetic Fields from the Photosphere to the Corona, ed. T. R. Rimmele et al. (San Francisco, CA: ASP), 107
Shelyag, S., Keys, P., Mathioudakis, M., & Keenan, F. P. 2011, A&A, 526, A5
Steiner, O., Franz, M., Bello González, N., et al. 2010, ApJL, 723, L180
van Noort, M., Rouppe van der Voort, L., & Löfdahl, M. G. 2005, SoPh, 228, 191
van Noort, M. J., & Rouppe van der Voort, L. H. M. 2008, A&A, 489, 429
Vargas Domínguez, S., Palacios, J., Balmaceda, L., Cabello, I., & Domingo, V. 2011, MNRAS, 416, 148
Verma, M., Steffen, M., & Denker, C. 2013, A&A, 555, A136
Wedemeyer, S., Scullion, E., Rouppe van der Voort, L., Bosnjak, A., & Antolin, P. 2013, ApJ, 774, 123
Wedemeyer-Böhm, S., Scullion, E., Steiner, O., et al. 2012, Natur, 486, 505
Withbroe, G. L., & Noyes, R. W. 1977, ARA&A, 15, 363
Zhou, J., Adrian, R. J., Balachandar, S., & Kendall, T. M. 1999, JFM, 387, 353